Geoderma 465 (2026) 117658

Contents lists available at ScienceDirect

Geoderma

journal homepage: www.elsevier.com/locate/geoderma

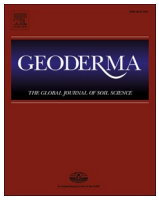

Root organic exudate stimulation of greenhouse gases is offset by radial oxygen loss in mineral-dominated anoxic wetland soil

Marie Mollenkopf [a,b,c], Ida Lena Haas [a], Andreas Kappler [a], E. Marie Muehe [b,c,*]

[a] Geomicrobiology, Department of Geosciences, University of Tübingen, Tübingen, Germany
[b] Plant Biogeochemistry, Helmholtz Centre for Environmental Research -UFZ, Leipzig, Germany
[c] Plant Biogeochemistry, Department of Geosciences, University of Tübingen, Tübingen, Germany

ARTICLE INFO

Handling Editor: Dr. Andrew Margenot

Keywords:
Root traits
Methane oxidation
Rusty carbon sink
Priming
Fermentation

ABSTRACT

Wetlands are important contributors to global CH_4 emissions, yet uncertainties remain regarding plant-mediated controls of greenhouse gas (GHG) fluxes. Wetland graminoids influence these emissions via multiple pathways. The study focuses on two key root traits: organic carbon exudation and radial oxygen loss (ROL). Their individual and combined impacts on soil organic carbon (SOC) dynamics and GHG emissions were investigated in 26-day-long incubations, using an anoxic mineral-rich permafrost fen soil as a wetland proxy. Organic exudation was imposed by repeated injection of an artificial organic compound mix mimicking real root exudate, and ROL by continuous ambient-air injection. Organic exudation enhanced CO_2 and CH_4 emissions 3- and 2.2-fold, respectively. This stimulated fermentation, methanogenesis, and Fe mineral dissolution, thereby co-mobilizing SOC from the 'rusty carbon sink'. ROL promoted methanotrophs and aerobes reducing bioavailable carbon pools, so that 29% less CO_2 and 47% less CH_4 were emitted compared to the no-addition control. The combination of organic exudation and ROL increased CO_2 by 70% and decreased CH_4 by 20% relative to the no-addition control, indicating active methanotrophs. Thus, Fe-associated OC increased ~4.6-fold with an OC:Fe ratio above 1, suggesting a persistent 'rusty carbon sink' with less bioavailable SOC. This study demonstrates that combined root traits can exert opposing effects on CO_2 and CH_4 emissions, which can improve prediction and management for natural, agricultural, and restored wetlands.

1. Introduction

Wetlands are the largest natural source of CH_4 and can either act as sinks or sources of CO_2 (Lafleur, 2009). These ecosystems range from thawing permafrost peatlands, flooded rice paddies, coastal salt marshes, and natural and restored temperate peatlands. They are characterized by steep redox gradients that regulate biogeochemical cycling and greenhouse gas (GHG) emissions (Reddy et al., 2022; Verhoeven and Sorrell, 2010). Through their growth and litter inputs, plants act as ecosystem engineers that shape redox potentials, microbial communities, and organic matter turnover (Laanbroek, 2010; Li et al., 2024; Mueller and Megonigal, 2024; Tanner, 2001; Verhoeven and Sorrell, 2010). Consequently, redox shifts can drive climate feedbacks, yet projections of CH_4 fluxes remain uncertain due to limited mechanistic understanding at fine spatial scales (Yazbeck and Bohrer, 2023). In this context, root traits represent key plant characteristics that govern biogeochemical heterogeneity at the soil-root interface (Bodelier, 2011; Lamers et al., 2012). In particular, the root traits radial oxygen loss (ROL) and root organic carbon (OC) exudation determine soil oxygenation and carbon (C) supply (Bodelier, 2011; Sutton-Grier and Megonigal, 2011).

Root organic exudation (hereafter termed organic exudation) is a major pathway by which plants affect soil processes. Up to half of the photosynthetically fixed C can be released into the rhizosphere as organic exudates, especially in high-yielding wetland graminoids (Hütsch et al., 2002). These organic exudates are diverse, low-molecular-weight OC containing substrates that serve as a fresh C source for soil microorganisms. Laboratory and field studies have demonstrated that added labile C can trigger a rhizosphere priming effect (RPE). RPEs are short-term shifts in microbial activity that change the mineralization of native soil OC (SOC) to CO_2 and CH_4 (Kuzyakov, 2010). In wetlands, priming has received less attention compared to uplands but can be of importance, with effects on CO_2 emissions ranging from suppression (−92%) to stimulation (+1242%) (Mueller and

* Corresponding author at: Marie Muehe, Plant Biogeochemistry UFZ Leipzig, Permoserstraße 15, 04318 Leipzig, Germany.
E-mail address: marie.muehe@ufz.de (E.M. Muehe).

https://doi.org/10.1016/j.geoderma.2025.117658
Received 29 August 2025; Received in revised form 19 November 2025; Accepted 14 December 2025

Megonigal, 2024). Organic exudates often stimulate not only CO_2 but also CH_4 emissions by rapidly depleting alternative electron acceptors and producing fermentation intermediates for methanogens (Waldo et al., 2019). The direction and extent of priming are controlled by soil properties such as pH and SOC content in combination with the root exudate composition (Mueller and Megonigal, 2024; Wang and Kuzyakov, 2024; Wild et al., 2023). Here, chelators within organic exudates were shown to mobilize iron (Fe) through complexation, co-mobilizing OC and thereby stimulating CO_2 release (Keiluweit et al., 2015). Yet, this process may thermodynamically inhibit methanogenesis when Fe(III) serves as electron acceptor (Van Bodegom et al., 2004). Preferential substrate use (Boye et al., 2017; Mueller and Megonigal, 2024) or the exhaustion of electron acceptors (Mueller and Megonigal, 2024) proved important to induce negative priming in wetland soils. The latter limitation can be alleviated by rhizosphere oxygenation via ROL (Krüger et al., 2025).

O_2 is photosynthetically produced in plant shoots, transported via aerenchyma from shoots to roots, and released into the rhizosphere in a process termed ROL (Colmer and Voesenek, 2009). As an adaptive trait to soil anoxia, ROL is characteristic of many wetland macrophytes (e.g., *Phragmites*) and wetland crops such as rice. The magnitude of ROL varies with species, light, phenological stage, and barriers to diffusion (Jimenez et al., 2021). ROL can create oxic hotspots that relieve anoxic constraints on complex OC breakdown, boosting CO_2 emissions (Krüger et al., 2025) and providing methanogenic substrates after O_2 depletion (Wilmoth et al., 2021). Mechanistically, ROL re-oxidizes Fe(II) forming root-associated Fe(III) plaques. Iron plaque refers to Fe(III)-(oxyhydr) oxide coatings that precipitate on root surfaces when ROL oxidizes Fe (II)-rich porewater (Maisch et al., 2020; Weiss et al., 2003). Such formation of Fe plaque can drive the adsorption and co-precipitation of dissolved organic carbon (DOC) forming the so called “rusty C sink” (Sun et al., 2025; Wei et al., 2022). DOC is thus protected from rapid mineralization. This protection can be dynamic: ligand-driven mineral dissolution or reductive dissolution during anoxic periods can remobilize previously stabilized OC (Li et al., 2021; Patzner et al., 2020). Furthermore, ROL regenerates terminal electron acceptors (i.e., Fe(III), Mn(IV), and O_2 itself) and thereby shifts redox pathways and alters both the type and amount of emitted GHGs, as electron donors are oxidized after bulk O_2 depletion (Agethen et al., 2018; Määttä and Malhotra, 2024). In this way, ROL can suppress methanogenesis by raising redox potentials to ranges inhibitory to methanogens and enabling Fe(III), Mn (IV), and nitrate reducers to outcompete methanogens for preferred substrates. ROL can enhance CH_4 oxidation by creating oxic layers around roots that stimulate CH_4-consuming methanotrophs (Vogel, 2017). In peat soils, ROL can promote positive priming (Krüger et al., 2025) and CH_4 formation (Wilmoth et al., 2021), while in mineral soils, stronger Fe-OC associations and plaque-mediated sorption may favor OC preservation and negative priming (Sun et al., 2025). Thus, the quantity and composition of root C exudates interact with the extent of ROL to control the balance of CO_2 and CH_4 fluxes in wetland soils (Haviland and Noyce, 2024; Krüger et al., 2025), and the direction of the combined effect may be further controlled by wetland soil properties (Mueller and Megonigal, 2024).

Most studies have isolated either ROL or organic exudation under simplified laboratory conditions to assess mechanisms, e.g., the direction and magnitude of ROL on CH_4 emissions. Key uncertainties towards the interactive effects of both organic exudation and ROL remain that limit predictions: (i) how exudate chemistry amplifies or counteracts ROL effects on Fe cycling and the rusty C sink, (iii) the persistence of plaque-stabilized OC under fluctuating redox conditions as well as, (iii) the net effect on microbial functional genes involved in GHG cycling.

In this study, both traits were applied concurrently to regulate CO_2 and CH_4 fluxes in microcosms containing field-sampled, anoxic, mineral-dominated wetland soil. An artificial root was used to mimic a low-redox rhizosphere for precise injection of O_2 and organic exudates. Four treatments were applied: (i) artificial rainwater (non-addition) control, to quantify net plant-trait effects, (ii) organic exudate solution of field-relevant composition and dose (iii) O_2 as ambient air to represent ROL, and (iv) the combination of organic exudates and O_2. The organic exudate mixes reflected graminoid metabolites measured from Stordalen Mire, Sweden, and ambient air reproduced realistic O_2 delivery. We hypothesized that combined organic exudation and O_2 addition increases CO_2 but decreases CH_4 emissions relative to organic exudate addition alone. By linking GHG measurements with root-surface soil and solution geochemistry assessments (C and Fe) and CH_4-cycling gene quantification, trait interactions under realistic substrate and O_2 regimes were isolated to inform wetland GHG predictions and management.

2. Materials and methods

2.1. Soils and simulated root-derived inputs

Mineral soil was sampled from a fen peatland soil in Stordalen Mire (68.35°N, 19.05°E), Abisko, Sweden. Stordalen is a well-studied Arctic permafrost peatland and is described elsewhere (Freire-Zapata et al., 2024). Samples were taken in September 2023 (Fig. S1) and stored anoxically and wet at 4 °C in the dark until the experiment started. Soil was chosen from a deeper layer for two reasons: (1) Graminoid root tips typically grow to the thaw front, (2) handling soil of a lower peat content for experimental purposes is easier. Soil was characterized prior to experimentation (Method S1).

The composition of the artificial organic exudation mix was based on OC released by graminoids, specifically *Eriophorum angustifolium* and *Carex* spp., from Stordalen mire in a hydroponic solution described in Oburger and Jones, 2018 (Fig. S2, Method S2). Based on this characterization, artificial organic exudates include malate (48%) and citrate (6%) as organic chelators, acetate (8%) as an organic acid known as an important exudate from graminoid roots (Meier et al., 2021), glucose as a common sugar (23%), and glycine (15%) representing amino acids and a nitrogen (N) source.

2.2. Experimental setup and sampling

Plastic tubes (250 mL) (HCl-, ultrapure water washed and UV-sterilized) were equipped with an ultrapure water washed pumice stone (1.5x2.5 cm, Pawly) imitating a root (Fig. S3B). A tube was connected to the artificial root equipped with a backflush valve (⌀ = 5 mm, Pawly) for ambient air and/or organic exudates injection. To sample porewater, an ultrapure water washed Rhizon sampler (Rhizosphere Research Products, Netherlands, standard Rhizon sampler MOM, 0.15 μm pore size) was mounted to the tube 1 cm above the pumice stone. 60 g of sieved (2 mm) soil and 20 mL of artificial rainwater (0.07 mM NaCl, 0.02 mM $NaHCO_3$, 0.02 mM K_2SO_4, 0.76 mM $CaSO_4$) were filled into the tubes. To acclimate to lab conditions, the soil was incubated anoxically for a 2.5-week pre-incubation. For establishing anoxic conditions, the tubes were closed gas-tight, and the headspace was flushed with N_2 several times. The experiment was set for four treatments: a control of adding artificial rainwater only (hereafter termed “(no-addition) control”), an O_2-only treatment continuously injecting ambient air as a realistic simulation of O_2 exudation (hereafter termed “O_2 exudation”, or “O_2” in figures), an artificial root C exudation treatment only (hereafter termed “organic exudates” or “OrgC” in figures), and a combination of O_2 and artificial C exudation treatment (hereafter termed “combined treatment”, or “O_2 + OrgC” in figures). Ambient air (~21% O_2) was used to mimic aerenchyma gas composition, rather than pure O_2. Additionally, all treatments were treated with artificial rainwater to balance the ionic strength.

Root density was set to 4.2 g dry root L^{-1} soil, informed by field measurements of graminoid roots from an adjacent permafrost peatland (Monteux et al., 2018) (Tab. 1). O_2 exudation rates were parameterized from literature of different wetland plants (Tab. 1) (Li et al., 2011),

Table 1
Specifics of treatment deliveries: Parameterization of root-mediated oxygen and carbon inputs in microcosm incubations using mineral-dominated fen soil.

Item	Value	Units	Notes/Source
Soil volume per microcosm	27.5	mL	From setup
Root density (dry)[#]	4.2	g L^{-1} soil	Field-based (adjacent permafrost peatland)[a]
ROL			
ROL reference rate[#]	0.07	mM O_2 h^{-1} g^{-1} dry root	Literature value across wetland plants[b]
Air pulsing schedule	7/15	s air/s cycle	Ambient air through artificial root
Weekly O_2 delivered (per replicate)	0.042	mM O_2 $week^{-1}$	From pulsing + parameterization *(as reported)*
Organic exudation			
Organic exudation reference rate[#]	16.3	mM C $week^{-1}$ g^{-1} dry root	From Stordalen graminoids, method adapted from (Oburger and Jones, 2018)
Organic exudation volume	2.6	mL	per injection
Weekly C input (per replicate)	1.88	mM C $week^{-1}$	Derived from rate × root density × soil volume
Injections per week	3	count	Evenly spaced

[#] Based on field measurements and literature values, used to derive weekly O_2 and organic exudation deliveries.
[a] Monteux et al., 2018.
[b] Li et al., 2011

assuming continuous ROL (24 h day^{-1}). Because ROL varies among species (e.g., Li et al., 2011) and site-specific data are limited, O_2 injection via the artificial root was set near the upper bound of reported graminoid ROL due to pump-diffuser stability constraints; this may overestimate field rates. Ambient air was injected in pulses every 15 s for 7 s, totalling 0.042 mM O_2 $week^{-1}$ per replicate. Root C exudation rates were based on hydroponic measurements of graminoids from Stordalen mire (adapted from Oburger and Jones, 2018), assuming exudation over a typical daily plant activity of 14 h. With the given root density and soil volume (27.5 mL), this resulted in a weekly input of 1.88 mM C per replicate, performed in three equal injections (2.6 mL each). Each treatment had five replicates (Fig. S3C).

For porewater sampling, porewater was withdrawn through the Rhizon into gas-tight syringes by applying a gentle vacuum, discarding the first ~ 0.5 mL and then collecting up to 5 mL per sampling. Samples were taken 2–3 × per week and sample water refilled with artificial rainwater to maintain volume/ionic strength. For Fe speciation, subsamples were transferred to headspace-free vials and immediately acidified to pH ≈ 0 with 1 M HCl to prevent Fe(II) oxidation; Fe_{tot} and Fe(II) were later measured by ferrozine. Porewater pH and $SUVA_{254}$/DOC were measured from the same Rhizon porewater (pH measured promptly after extraction; DOC/SUVA filtered through Rhizon). All porewater measurements thus refer to Rhizon-extracted porewater 1 cm above the artificial root, not bulk slurry.

For GHG quantification, the tube headspace was flushed with N_2, and subsequently, 3 mL of headspace gas was taken after 2, 20, and 40 min and transferred to a 12 mL pre-N_2-flushed exetainer. Gas was sampled every second to third day. Porewater was extracted 2–3 times per week via the Rhizon with max. 5 mL per sampling and refilled with artificial rainwater. Collected porewater was subsequently aliquoted for geochemical analyses, including pH, DOC, and N species, Fe speciation, and OC aromaticity. To protect Fe(II) from oxidation, samples were stored by acidifying with 1 M HCl to a pH of 0.

In a final sampling, tubes were sawed open. Sequential Fe and OC extraction was performed with the artificial roots after washing in ultrapure water. For this, the stone was sequentially put into 0.5 M and 6 M HCl and extracted for 30 min and 24 h with 1:2.5 (w/v) ratio on a horizontal shaker (150 rpm), and aliquoted for Fe and DOC analyses. Soil (approx. 1 g) taken directly adjacent to the artificial root was shock-frozen at −80 °C for molecular biological analyses. A subsample was taken for water content.

2.3. Gas and aqueous analyses

GHG concentrations including CO_2 and CH_4 were quantified using gas chromatography (TRACE 1310, Thermo Fisher Waltham, Massachusetts, USA) equipped with two pulsed discharge ionization detectors (PDD) (N_2O was consistently below detection limits). Measured parts per million (ppm) concentrations were corrected for sampling temperature using the ideal gas law. Gas production rates were calculated based on a linear change in headspace gas concentration over time and normalized to g dry soil according to the equations published in Ruser et al., 1998. The warming potential (WP) of the sum of the two gases in CO_2-equiv. was calculated assuming gas-specific abilities of radiative efficiency and lifetimes in the atmosphere (amount of energy absorbed by 1 ton of gas over a given period relative to 1 ton of CO_2). CH_4 has a WP 27 times higher than CO_2 on a 100-year timeframe (Parada et al., 2016).

DOC was quantified in technical triplicates on a multi N/C 2100 (Analytik Jena, Germany). The Specific UV absorbance at 254 nm ($SUVA_{254}$) (Specord 50 plus, Analytik Jena, Germany) was used to represent the aromaticity of DOC. pH was determined with technical triplicates using an InLab Easy pH probe (Mettler Toledo, USA). Nitrogen species (nitrite, nitrate, and ammonium) were quantified in technical unicates using flow injection analysis (AA3, Seal analytical, USA). Total Fe concentrations and speciation were quantified in technical triplicates spectrophotometrically with the ferrozine assay after Stookey, 1970 (MultiskanTM GO, Thermo Fisher Scientific).

2.4. Soil microbial ecology analyses

DNA and RNA were co-extracted twice, before addition (day 0) and after the incubation (day 26), from soil (anoxic incubation) as described previously (Lueders et al., 2004) and 806-R (5′-GGACTACNVGGGTWTCTAAT-3′) (Apprill et al., 2015) followed by 1% (w/v) ethidium-bromide-died agarose gel.

Gene and transcript copy numbers were quantified with quantitative PCR (qPCR) using 1 × SsoAdvanced Universal SYBR Green Supermix (Bio-Rad Laboratories, Hercules, CA, USA) for 16S rRNA, and the functional genes for methanogenesis methyl coenzyme-M reductase *(mcrA)* and aerobic methanotrophs particulate methane monooxygenase *(pmoA)*. In a 10 µL reaction volume, 1 µL of template DNA and cDNA or a tenfold dilution series of the standard plasmid DNA were annealed gene-specific forward and reverse primers (Tab. S1). The qPCR programs ran on a CFX Connect Real-Time PCR Detection System (Bio-Rad Laboratories, Hercules, CA, USA). The data analysis was performed using the Bio-Rad CFX Maestro software (Bio-Rad Laboratories, Hercules, CA, USA). Transcript abundances (16S rRNA, *mcrA*, *pmoA*) were normalized to dry soil mass (per g dry soil). For the 16S rRNA genes and transcripts are presented to inform about potential cell numbers and their activity. For functional genes, the transcripts are presented to inform about their activity.

2.5. Data analyses

Means and one standard deviation (1SD) were calculated for all data except for molecular biology data, where standard errors (SE) were used. For whisker-boxplots, black diamonds represent the mean, and the line in the box is the median; whiskers show the 5th and the 95th percentile. Fold changes were calculated for most datasets and presented in percent, and when exceeding 100% as fold change.

Stabilization of root-exuded C in Fe-bound minerals, and the ratio of dissolved versus Fe–bound C, was calculated as detailed in Method S3.

Linear mixed models (LMMs) were used to assess the effects of organic exudate addition, O_2 addition, and their interaction on cumulative CO_2 and CH_4 emissions and on (functional) transcript abundances (*mcrA, pmoA,* 16S rRNA). Models were fit by restricted maximum likelihood (REML) and Type III sums of squares. Estimated marginal means (EMMs) are reported with Least Significant Difference (LSD) adjusted pairwise comparisons ($\alpha = 0.05$). Predefined, time-point-specific hypotheses were evaluated with two-sided, unpaired t-tests. Normality was assessed using Kolmogorov-Smirnov tests and variance homogeneity Levenés test; when assumptions were not met, appropriate non-parametric alternatives were applied. For all tests, statistical significance was defined as $p < 0.05$. Analyses were performed in SPSS Statistics v27 (IBM Corp., USA). For multivariate structure, Principal Component Analysis (PCA) was performed on standardized variables in R (v4.4.2 (R Core Team, 2024) using prcomp() in RStudio (2v2024.09.1+394, (Posit, 2024))), 80% confidence ellipses and loading vectors visualized using *ggplot2*, *ggrepel*, and *factoextra* (Kassambara and Mundt, 2020; Slowikowski, 2024; Wickham, 2016).

3. Results

The soil can be classified as Histosol (WRB), and the fixed 60 cm sampling depth targeted the gleyed mineral subsoil beneath the surface peat. The texture of the soil was silt-dominated (85 ± 6% silt, 12% sand, 12% clay; Tab. 2). The soil contained 1.22 ± 0.03% SOC and 0.05 ± 0.02% total N, with a C:N ratio of ~ 24, and had a slightly acidic pH (pH = 5.45). Organic matter was primarily mineral-associated (MAOC = 76.5%), while particulate organic carbon (POC) accounted for 17.3%.

3.1. Greenhouse gas dynamics during Incubation

CO_2 emissions from the no-addition control were 5.2 ± 0.1 mg CO_2 g^{-1} soil on day 1 and were stable over 26 days of incubation (Fig. 1A). The addition of organic exudates did not affect the CO_2 emissions until day 12, after which it led to the highest cumulative CO_2 emissions among all treatments. By day 26, organic exudates had increased cumulative CO_2 emissions 3-fold relative to the control. O_2 release reduced cumulative CO_2 emissions, with divergence from the control starting on day 8, and resulted in 29% less emitted CO_2 by the end of the experiment. The combination of O_2 release and organic exudation increased cumulative CO_2 emissions by 70% relative to the control, with divergence starting on day 19. However, total CO_2 emissions under this combined treatment remained lower than those observed with organic exudates alone, and an interaction was confirmed with LMM.

Table 2
Soil characteristics of the used soil sampled in Stordalen, Abisko, Sweden.

Parameters	Units	Fen soil
Coordinates (approx.)		68°21′15.4″N 19°02′41.5″E
Soil Type (WRB)		Histosol
Texture[c]		
Sand[c]	%	12 ± 0
Silt[c]	%	85 ± 6
Clay[c]	%	12 ± 0
SOC[a]	%	1.22 ± 0.03
Total N[b]	%	0.05 ± 0.02
POC[b,c]	%	17.3
MAOC[b,c]	%	76.5
pH (H_2O)		5.45
Active layer depth	cm	∞

[a] Soil Organic Carbon (SOC) and Nitrogen (Total N) in the dried and milled soil measured with a soli TOC cube (Elementar, Germany).

[b] Particulate organic C (POC) and Mineral-Associated Organic Carbon (MAOC) were assessed by extracting with 0.5% sodium hexaphosphate and subsequent size fractionation.

[c] Parameters were analyzed on soil collected at the same locations in July 2023 as compared to the soil collected in Sept 2023.

CH_4 emissions were 1.2 ± 0.4 mg CO_2-equiv. g^{-1} soil in the no-addition control on day 1 and stable during the experimental phase (Fig. 1B). The addition of organic exudates increased cumulative CH_4 emissions 2.2-fold relative to the control, with divergence apparent from day 4. O_2 exudation reduced cumulative CH_4 emissions by 47% relative to the control by the end of incubation, with divergence starting on day 8. The combined O_2 and organic exudation reduced CH_4 emissions by 20% relative to the control at the end of incubation, with divergence starting on day 8. The interaction of O_2 and organic exudation was confirmed with a LMM.

The CO_2:CH_4 ratio, averaged across all incubation timepoints, in the no-addition control soil was 52.5 ± 6.3 and increased 1.1-fold with organic exudates, 1.4-fold with O_2 exudation, and 2.6-fold with their combined addition (Fig. 1C). N_2O was not quantifiable in both oxic and anoxic incubations, supported by high porewater NH_4^+ (Fig. S7A). N_2O spikes usually appear early on after flooding, so emissions may have occurred during pre-incubation of the soil and prior to experimental start. Thus, N_2O data does not feed into warming potential calculations here.

The warming potential at the end of incubation of the no-addition control was 29.1 ± 5.3 mg CO_2-equiv. g^{-1} soil (Fig. 1D). Organic exudates increased the warming potential 2.9-fold, yet O_2 exudation tended to decrease the warming potential by 33% ($p = 0.068$). The combination of organic and O_2 exudation did not alter the warming potential significantly compared to the control, though a trend of 53% increase could be noted given high replicate variability ($p = 0.110$).

3.2. Fe and OC dynamics at the artificial root

"Reactive" Fe denotes 0.5 M HCl-extractable Fe (short-term pool), and "recalcitrant" Fe denotes 6 M HCl-extractable Fe (longer-term pool), which were sequentially extracted and can be related to the respective amount of trapped OC. In the no-addition control, root-associated reactive Fe_{tot} averaged 1.2 ± 0.1 μmol g^{-1} artificial root (Fig. 2A). O_2 exudation did not affect reactive Fe_{tot} compared to the control, while organic exudates decreased reactive Fe_{tot} by 74%. Their combination increased root-associated reactive Fe_{tot} by 88% relative to the control. The co-precipitated or adsorbed OC in the reactive Fe fraction was 1.4 ± 0.9 μmol g^{-1} artificial root in the control and increased in the order control < O_2 < organic exudates < combination. The combination had 4.6-fold higher reactive Fe-associated OC than in the control (Fig. 2B).

In the no-addition control, root-associated recalcitrant Fe_{tot} was 3.6 ± 0.3 μmol g^{-1} artificial root (Fig. 2A). Organic exudates did not change recalcitrant Fe_{tot}, whereas O_2 exudation increased Fe_{tot} 2-fold. The combination of organic and O_2 exudation increased recalcitrant Fe_{tot} 3.8-fold relative to the control. OC associated with the recalcitrant Fe mineral fraction averaged 12.6 ± 3.4 μmol g^{-1} artificial root (Fig. 2B). Organic exudates tended to increase the amount of root-associated, recalcitrant OC by 31% compared to the control. O_2 exudation and the combined treatment of organic and O_2 exudation increased OC by 50% and 2.6-fold relative to the control, respectively.

The linear regression ($R^2 = 0.891$, $p < 0.0001$) between Fe and OC concentrations reveals that adsorption occurs predominantly at lower Fe concentrations, whereas co-precipitation becomes more dominant at higher Fe concentrations, particularly under combined O_2 and organic exudation treatments (Fig. 2C). OC trapping efficiency and the dissolved-to-trapped OC ratio are both highest when organic exudates are present, with the combined treatment enhancing OC retention compared to individual treatments (Fig. 2D).

3.3. Microbial and geochemical response during incubation

Microbial gene/transcript data were collected on day 0 (pre-addition) and endpoint (day 26), whereas porewater chemistry (e.g., Fe, DOC, metabolites, pH) was monitored throughout via Rhizon samplers 1 cm above the artificial root. We summarize these trajectories and

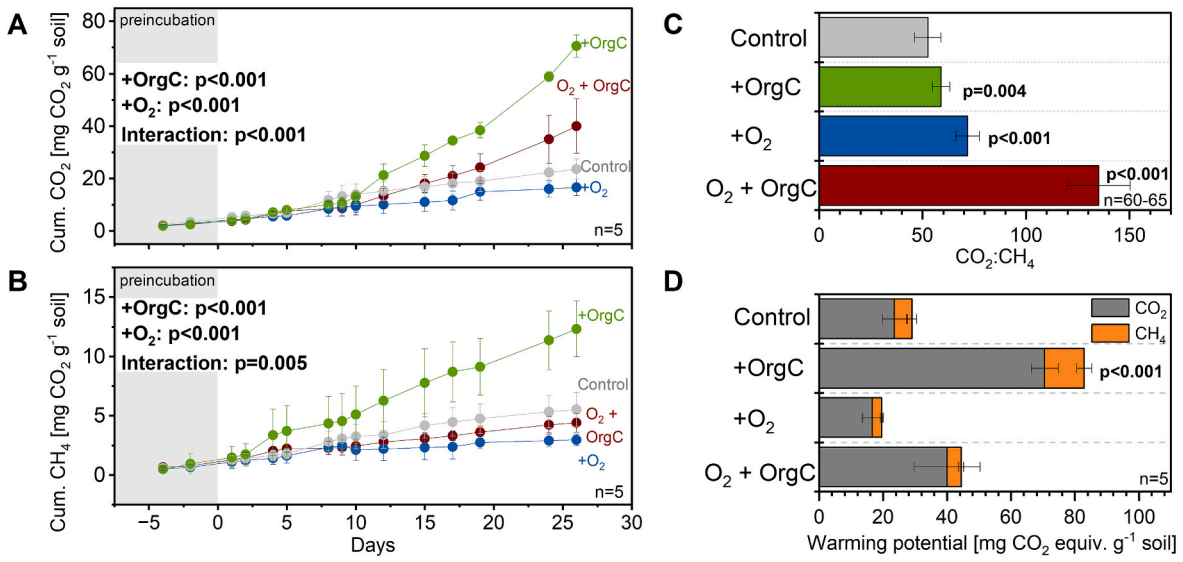

Fig. 1. Greenhouse gas emission from anoxic soil exposed to single or combined root traits. Greenhouse gas dynamics in anoxic microcosms containing mineral soil from a thawed permafrost fen peatland (Stordalen Mire, Abisko, Sweden). Soils were exposed to single or combined root traits: (1) no-addition control (Control, grey), (2) organic exudates (+OrgC, green), (3) O_2 release (+O_2, blue), and (4) combination of organic and O_2 exudation (O_2 + OrgC, red). Cumulative (A) CO_2 and (B) CH_4 emissions (in CO_2-equiv.) during incubation. (C) CO_2:CH_4 ratios based on molar concentrations over the whole incubation period after substrate additions. (D) Warming potentials based on cumulative emissions at the end of the incubation. For (A) and (B), significance was assessed using linear mixed models (LMM) with organic exudation, O_2 exudation, and their interaction as fixed factors (Tab. S2-3 for full statistics). For (C) and (D), significance was tested by a two-sided *t*-test or non-parametric alternatives when data were not normally distributed. Mean ± 1SD. Significance (two-sided t-tests or non-parametric alternative) included if $p < 0.05$, always tested for treated against control, full statistics see Tab. S4).

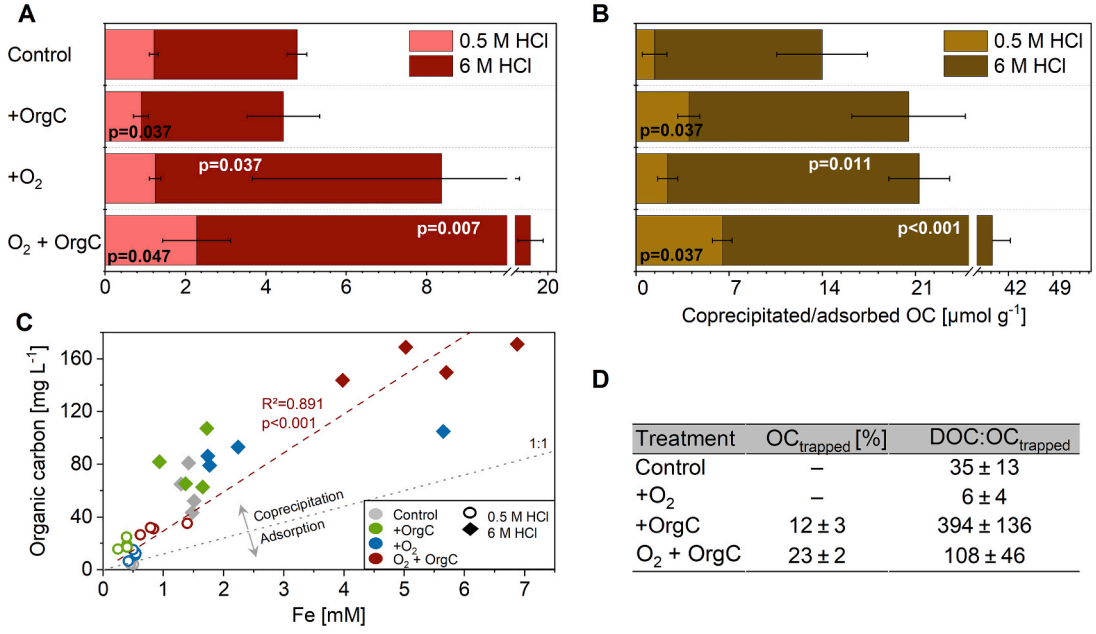

Treatment	$OC_{trapped}$ [%]	$DOC:OC_{trapped}$
Control	–	35 ± 13
+O_2	–	6 ± 4
+OrgC	12 ± 3	394 ± 136
O_2 + OrgC	23 ± 2	108 ± 46

Fig. 2. Artificial root plaque Fe and organic carbon in anoxic soils exposed to single or combined root traits. Artificial root plaque Fe and organic carbon (OC) dynamics in anoxic microcosms containing mineral soil from a thawed permafrost fen peatland (Stordalen Mire, Abisko, Sweden). Soils were exposed to single or combined root traits: (1) no-addition control (rainwater only), (2) organic exudates (+OrgC), (3) O_2 exudation (+O_2), and (4) combination of organic and O_2 exudation (O_2 + OrgC). (A) Fe and (B) OC determined by sequential extraction from the artificial root, separating reactive (0.5 M HCl extraction) from recalcitrant phases (6 M HCl extraction). Data represent mean ± 1SD, n = 4. Significance (two-sided *t*-test or non-parametric alternative) included if $p < 0.05$ in black for 0.5 M extraction, in white for 6 M HCl extraction, always tested for treated against control (Tab. S5). (C) Correlation between Fe and OC. The black dashed reference line at OC/Fe = 1 indicates when co-precipitation of Fe and OC dominates over adsorption (OC:Fe < 1) and vice versa (Chen et al., 2014). The red dashed line is the linear regression for all treatments. (D) The percentage of added OC captured in Fe-associated phases and the total porewater OC: Fe-trapped OC were calculated (see Method S3). Fe-associated OC refers to OC in Fe extracts and does not represent total mineral-associated OC.

endpoint responses in Fig. 3 and Figs. S4–S7.

Porewater Fe(II) in no-addition control soils averaged 0.11 ± 0.08 mM (Fig. 3A). Organic exudates increased Fe(II) 21.8-fold relative to the control, while O_2 exudation decreased Fe(II). The combined exudation of O_2 and organic exudates increased Fe(II) 7.4-fold compared to the control. Fe_{tot} and $Fe(II)/Fe_{tot}$ as well as porewater DOC followed these

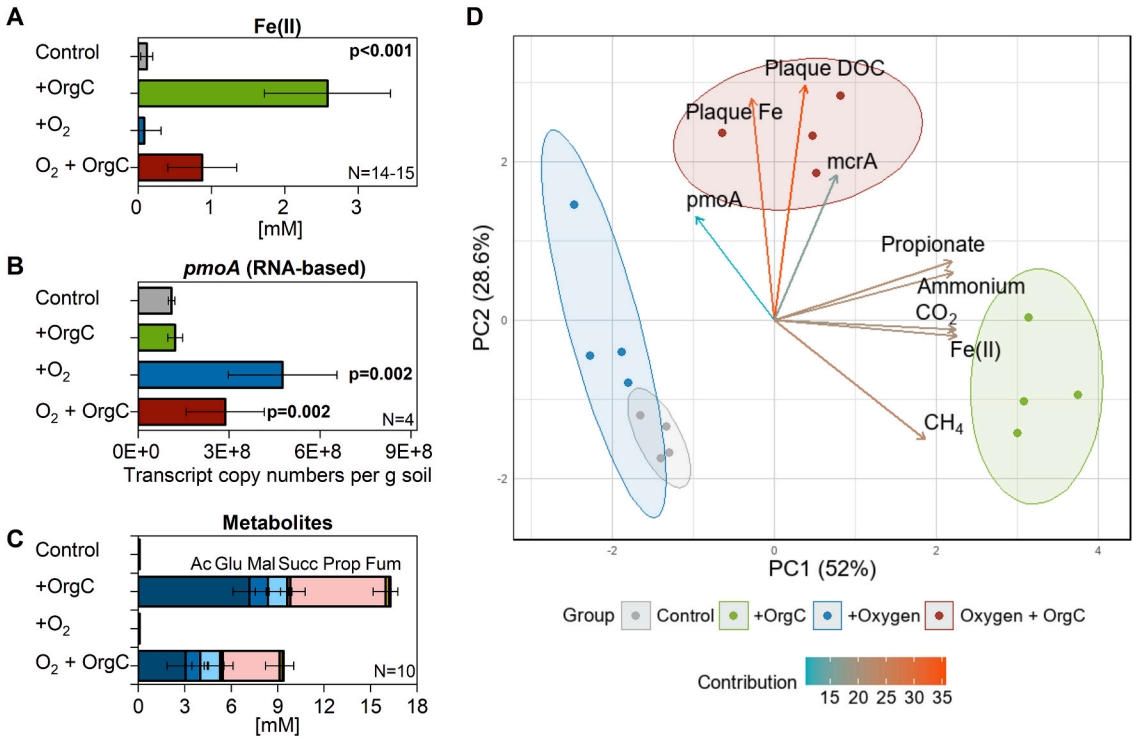

Fig. 3. Biogeochemical variables and principal component analysis (PCA) of microbial and geochemical patterns in anoxic soils exposed to single or combined root traits. Data was obtained from anoxic microcosms containing mineral soil from a thawed permafrost fen peatland (Stordalen Mire, Abisko, Sweden). Soils were exposed to single or combined root traits: (1) no-addition control (rainwater only, grey), (2) organic exudation (+OrgC, green), (3) O_2 exudation (+O_2, blue), and (4) combined organic exudate and O_2 exudation (O_2 + OrgC, red). Concentrations averaged from day 12 to the end of incubation of only at the end of incubation (B) are shown for (A) Fe(II), (B) transcript copy numbers of *pmoA*, and (C) metabolite concentrations (Ac = acetate, Glu = glucose, Mal = malate, Prop = propionate, Fum = fumarate). Bars represent means ± 1SD. Significance (two-sided t-tests or non-parametric alternative) included when $p < 0.05$, always tested for treated against control, full statistics in Tab. S6-7. Fe_{tot}, Fe(II)/Fe_{tot} and DOC/SUVA in Fig. S4-5, DNA-based/RNA-based functional gene copy and transcripts of 16S rRNA, *mcrA*, *pmoA* in Fig. S6. (D) PCA biplot illustrates the clustering of treatments based on microbial and geochemical variables. Ellipses represent 80% confidence intervals. Arrows indicate the loadings of selected microbial (*pmoA*, *mcrA* transcripts) and geochemical (e.g., plaque on (DOC, 0.5 M + 6 M HCl extracted), ammonium) variables driving the separation along principal components.

patterns (Fig. S4). DOC aromaticity ($SUVA_{254}$) increased in the combined treatment relative to the control, differing from Fe /DOC patterns (Fig. S4C).

16S rRNA, *mcrA,* and *pmoA* functional gene copy quantification marginally changed with root trait treatments (Fig. S6, top). The only notable change in absolute gene abundance was observed for *pmoA*, which decreased by 81% under organic exudate addition compared to the control (Fig. S6C). For the aerobic CH_4 oxidation gene *pmoA*, organic exudates did not affect transcript numbers, whereas both O_2 exudation and the combined treatment increased *pmoA* 4.3- and 2.6-fold, respectively, compared to the control (Fig. 3B, Tab. S6C). In contrast, CH_4 production gene *mcrA* transcripts significantly increased 17-fold under organic exudates alone, 7.1-fold under O_2 exudation, and increased 143-fold under the combined addition, differing from the *pmoA* response (Fig. S6E). 16S rRNA transcripts increase under all treatments, with the highest, 7.5-fold increase in the combined addition relative to the control (Fig. S6D).

Organic metabolites in the porewater, indicative of active microbial processes such as fermentation, were quantified (Fig. 3C). Soils with added organic exudates contained the highest total metabolite concentrations (16.3 ± 4.1 mM), which decreased by 42% under the combination of organic and O_2 exudation. Individual metabolites were distinctly affected by the combined treatment. While citrate, malate, and succinate concentrations did not differ under combined conditions compared to the organic exudate addition, others, such as propionate and acetate, substantially decreased by 40%, and 57%, respectively. For both control and O_2 exudation, metabolites were below the detection limit.

Based on the PCA, organic exudation positively correlated with dissolved Fe(II), ammonium, CO_2, and CH_4 emissions as well as propionate concentrations (Fig. 3D). O_2 exudation positively correlated with *pmoA* transcript abundance, while the combined addition correlated with plaque-associated DOC and Fe, as well as both *mcrA* and *pmoA* transcripts. Compared to the control, transcript abundances were 4.3-fold and 2.6-fold higher for *pmoA* under O_2 and combined treatments, and 17-fold, 7.1-fold, and 143-fold higher for *mcrA* under organic exudate, O_2, and combined additions, respectively. These changes co-occurred with lower and higher end-point CH_4 totals (Fig. 3B; Fig. S6E; cf. Fig. 1B).

Porewater NH_4^+ in the no-addition control was 0.24 ± 0.12 mg L^{-1} (Fig. S7A). Organic exudates increased NH_4^+ 135-fold relative to the control, while O_2 exudation increased NH_4^+ 9-fold. The combination of organic and O_2 exudation increased NH_4^+ 80-fold compared to the control. Porewater NO_3^- in the no-addition control averaged at 52.0 ± 3.8 µg L^{-1} (Fig. S7B). Only organic exudates increased NO_3^- by 24% compared to the control, while O_2 exudation and the combination of organic and O_2 exudation did not affect NO_3^- concentrations (Fig. S7B).

Porewater pH in the no-addition control averaged 5.45 ± 0.16 during the preincubation and varied slightly over time (Fig. S7C). Organic exudates decreased pH by 2 units directly after the experiment started but recovered almost to control levels over time. O_2 exudation decreased pH by up to 0.7 after the experiment started. The combination of organic and O_2 exudation initially decreased pH by 1.7 units, and pH remained 0.3 units lower than the control on day 14.

4. Discussion

Repeated additions of organic exudates and O_2 resulted in distinct microbial and geochemical soil responses that depend on root trait combinations, as indicated by their separation in the PCA ordination (Fig. 3D). Organic exudation, O_2 release, and their interaction significantly influenced microbial CO_2 and CH_4 emissions and selected functional genes, as confirmed by the LMMs (Fig. 1, Tab. S2-3, Fig. S6, Tab. S8–10). The combined addition of organic exudates and O_2 to this mineral soil with low SOC and high MAOC (Tab. 2) decreased the overall warming potential compared to organic exudation alone, consistent with a strengthened Fe-oxide "rusty C sink" and elevated activity of CH_4 oxidizers (conceptualized in Fig. 4). These findings highlight the importance of root trait combinations, particularly the interactive effect of organic exudation and O_2 release, for wetland C cycling alongside hydrology and SOC quantity and quality. In the following, we separate the discussion into two parts, one on the effects of organic exudates and O_2 release, and the other on specific effects of their combination.

4.1. *Organic exudates and O_2 release altered microbial and geochemical soil responses in opposite directions*

Three linked mechanisms drove alterations in CO_2 and CH_4 emissions: (1) Fe-OC interactions, (2) shifts in OC decomposition pathways, and (2) opposing activity of methanogens and methanotrophs (illustrated in Fig. 4).

Organic exudates containing low-molecular-weight carboxylates like malate and citrate likely promoted ligand-induced dissolution of Fe(III) minerals (Fig. 3A). In line with the findings of others (Keiluweit et al., 2015; Li et al., 2021), this process would co-mobilize associated OC and increase the availability of aromatic DOC (Fig. S4). In such anoxic systems, mobilized Fe(III) and OC can fuel fermentation and more Fe(III) reduction, alleviating energetic constraints on anaerobic respiration (Duchesneau et al., 2025). Given that 77% of SOC in this soil was MAOC, mobilization of Fe-associated OC likely accessed a substantial mineral-bound pool (Voggenreiter et al., 2024), even though the sequential extractions used here do not isolate the Fe-specific fraction of MAOC.

Parallel to Fe(III) reduction, organic exudates altered N cycling. Organic-exudate-derived glycine was efficiently mineralized, with approximately 20% recovered as NH_4^+, whereas NO_3^- accumulation remains minimal (<0.1%, Tab. S11, Fig. S7B). This pattern is consistent with ammonification as a major anaerobic pathway, providing additional electron donors (Jeannotte, 2014) and only minor heterotrophic nitrification in localized microsites. The resulting increase in reduced N further supported microbial growth and activity under organic exudate addition.

These geochemical shifts translated into distinct microbial responses. Organic exudates stimulated overall microbial activity, as reflected in higher 16S rRNA transcripts, and favored anaerobic decomposers and methanogens. The substantial increase in *mcrA* transcripts under organic exudate addition, combined with elevated fermentation products and higher CH_4 emissions, indicates efficient channeling of organic exudate-derived and mobilized C into methanogenesis (Fig. 1B, Fig. 3C, Fig. S6E) (Waldo et al., 2019; Wild et al., 2016). The temporal pattern, with early divergence of CH_4 trajectories and delayed CO_2 increases, together with relatively low CO_2/CH_4 ratios, suggests a prominent contribution of hydrogenotrophic methanogenesis. Acetoclastic methanogenesis, being more sensitive to initial acidic, Fe(III) reducing conditions (Hattori, 2008; Lovley and Phillips, 1987) was likely limited at first. As pH partially recovered and DOC aromaticity declined later in the incubation (Fig. S5, Fig. S7C), conditions became more favorable for a broader set of methanogenic pathways.

In contrast, simulated O_2 exudation mimicking ROL, reduced both CO_2 and CH_4 emissions relative to the no-addition control (Fig. 1). Continuous O_2 supply supported (1) the formation of Fe (oxyhydr)oxides as plaques around the artificial root, (2) enhanced Fe-associated OC, and (3) stimulated methanotrophs, as indicated in Fig. 4. The formation of a persistent Fe root plaque is supported by increased both reactive and recalcitrant Fe pools (Fig. 2), and its association with OC indicates effective trapping of DOC and reduced substrate availability for anaerobic respiration (Fig. 2, Fig. S4, Fig. S5). This is consistent with the formation of a "rusty C sink" in mineral soils (Chen et al., 2014; Zhu et al., 2023). Lower Fe(II)/Fe_{tot} ratios indicate thermodynamic suppression of methanogenesis, while increased *pmoA* transcript abundance and lower CH_4 emissions demonstrate stimulation of methanotrophic activity with efficient CH_4 oxidation in oxygenated microsites (Bian et al., 2020; Noyce et al., 2023; Teh et al., 2005).

The response to O_2 addition contrasts with findings from high-SOC peat soils, where O_2 inputs accelerated aerobic decomposition and increased CO_2 release, as shown by Krüger et al., 2025. In the low-SOC, mineral-dominated soil studied here, strong Fe-OC interactions favored incorporation and stabilization of C in Fe mineral phases and microbial biomass rather than increased respiratory CO_2 losses. Suppression of strictly anaerobic pathways could have further contributed to lower CH_4 emissions under O_2 supply. Together, the single-trait treatments show that organic exudation in mineral anoxic soil amplifies fermentation, Fe(III) reduction, and methanogenesis, whereas O_2 release reinforces Fe-bound C stabilization, constrains methanogenesis, and promotes methanotrophy (Fig. 4).

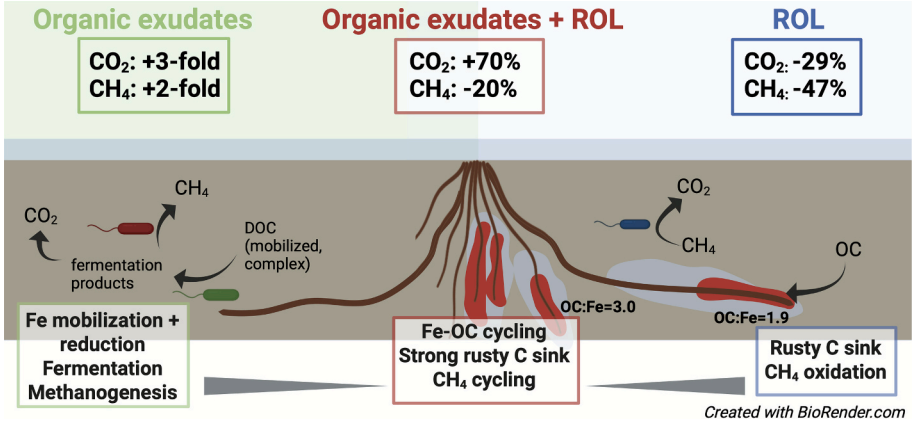

Fig. 4. Conceptual understanding derived from the present study how individual and combined root traits, namely organic exudation and O_2 release, regulate the rusty carbon sink and associated greenhouse gas emissions. Red: formed iron plaque around roots, light blue: O_2 released from roots. OC:Fe values represent the ratios of OC to Fe in iron plaque using the reactive Fe fraction (targeted in a 0.5 M HCl extraction).

4.2. Interactive impacts of organic exudates and O_2 release on the rusty C sink and related GHG dynamics

The combination of organic exudation and O_2 release decreased CH_4 emissions by 20% relative to the control, while it increased CO_2 emissions by 70% (Fig. 1, conceptualized in Fig. 4). These outcomes were not predictable from single-trait effects alone and reflect coupled Fe-OC dynamics and active CH_4 cycling. Here, repeated cycles of organic exudate-driven Fe dissolution and O_2-driven re-precipitation at the artificial root surface enhanced plaque growth and Fe-associated OC trapping compared to single-trait treatments (Fig. 2A–C, Fig. S4).

Under combined inputs, both reactive and recalcitrant Fe pools increased, and OC bound to these phases was substantially enriched (Fig. 2). OC:Fe ratios larger than one indicate that co-precipitation dominated over adsorption, forming a more stable Fe-bound C pool and supporting the concept of a more persistent rusty C sink (Chen et al., 2014; Bhattacharyya et al., 2018) (conceptualized in Fig. 4). The combined treatment trapped nearly twice as much OC in Fe-associated phases as organic exudates alone (Fig. 2D), which reduced the fraction of added and mobilized OC available for mineralization. Cumulative CO_2 emissions thus remained lower than in the organic exudate-only treatment despite sustained inputs of labile substrates. These results are consistent with the idea that O_2-driven plaque formation can stabilize organic exudate-derived OC and MAOC when both traits co-occur.

At the same time, combined organic exudation and O_2 release stimulated multiple microbial processes. Fermentation products and elevated ammonium confirmed active decomposition and N mineralization (Fig. 3C, Fig. S7, Tab. S11). The transcript of *mcrA* and *pmoA* increased under the combined treatment (Fig. 3B, Fig. S6E), indicating that methanogenesis and CH_4 oxidation were simultaneously stimulated. The net outcome of reduced CH_4 emissions despite increased methanogenic potential implies efficient CH_4 recycling within oxygenated and Fe-rich microsites, where methanotrophs and alternative electron-accepting processes limit the escape of CH_4 to the headspace. Thus, the combined traits support strong internal CH_4 cycling in combination with a strengthened rusty C sink (Fig. 4).

The porous artificial root used here mimicked organic exudation and ROL and induced controlled plaque formation, but it did not capture full rhizosphere biology, including root growth, exudate turnover at the root surface, and plant uptake. The experiment is therefore best interpreted in terms of process contrasts among treatments rather than absolute plant fluxes. Nevertheless, the observed non-additive behavior demonstrates that predictions based solely on single traits risk misrepresenting wetland Fe-C-CH_4 interactions. The results emphasize that the rate and composition of organic exudation, the magnitude and spatial pattern of ROL jointly define whether mineral-dominated anoxic soils act as net sources or partial sinks for exudate-derived C and CH_4. Precise consideration of interacting root traits and Fe-mediated stabilization is therefore essential for projecting CO_2 and CH_4 dynamics in thawing permafrost wetlands, agricultural wetlands, and restored systems where roots increasingly occupy mineral horizons.

4.3. Ecological implications

Wetland root traits control wetland C processes, yet the combination of root traits can exert opposing outcomes in terms of GHG emissions. These findings are relevant to both natural and managed wetlands, including agricultural and restored systems, where combining organic exudation with ROL can lead to decreased CH_4 emissions while stabilizing OC. In this study, organic and O_2 exudation were implemented at realistic concentrations based on field measurements (organic exudates) and O_2 release rates of different wetland species (Li et al., 2011). However, it is important to recognize that these root traits exhibit substantial variability both intra- and interspecifically, as well as under different environmental conditions, including diurnal and seasonal dynamics. In addition, the magnitude and composition of both organic and O_2 exudation can vary strongly with root type (e.g., young vs. mature roots, active vs. structural roots) and with the plant's developmental stage. Moreover, differences in diffusion kinetics between gaseous O_2 and dissolved organic exudates imply distinct spatial and temporal scales of influence around roots (York et al., 2016). Rapid O_2 diffusion creates sharp but spatially limited oxidizing zones, while slower diffusion of dissolved organics likely generates broader, longer-lasting impacts on microbial processes. Understanding these dynamics is essential for accurately predicting root trait interactions and their consequences for GHG emissions. Our findings from mineral-dominated, low SOC soils suggest that stimulatory effects could be overstated if research exclusively considers organic exudation without concurrent O_2 exudation. Vascular plant roots are expected to grow further downward following warming-induced deepening of active layers (Blume-Werry et al., 2019), thus reaching soil horizons with lower SOC contents compared to surface peat soils. Considering this and that ROL predominantly occurs at root tips, studies on wetland plant root traits should not solely focus on organic-rich peat. Root traits constitute a primary axis of wetland C cycling (Määttä and Malhotra, 2024) alongside hydrology and SOC quantity/quality. Considering their combined expression is therefore crucial for predicting CO_2 and CH_4 outcomes.

Future studies should thus systematically assess how different combinations of organic exudation and O_2 release influence GHG emissions across soil types and plant or root densities. Ultimately, understanding plant species-specific variations in organic and O_2 exudation under changing environmental conditions, such as fluctuating water levels, seasonal variability, and climate-induced warming, will increase our capacity to predict and manage wetland contributions to global climate change. With this, the present findings add information with ecological implications across different wetland ecosystems, e.g. (1) to help estimate and predict C processes and GHG release from expanding thawed permafrost (Christensen, 2024), and (2) to manage restored and agricultural wetlands where the precise knowledge of the effect of combined root traits will help develop strategies to reduce GHG emissions, e.g., through optimizing conditions for C sequestration or minimizing CH_4 release. By accounting for interacting root traits, the results refine projections of CH_4 fluxes under climate warming, particularly as roots penetrate mineral horizons with distinct redox and C conditions. Management should prioritize plant species or mixtures with a high ratio of ROL to organic exudation and maintain water levels that sustain thin oxic zones around root tips promoting Fe-oxide plaque formation and CH_4 oxidation.

CRediT authorship contribution statement

Marie Mollenkopf: Writing – review & editing, Writing – original draft, Visualization, Validation, Project administration, Methodology, Investigation, Funding acquisition, Formal analysis, Data curation, Conceptualization. **Ida Lena Haas:** Writing – review & editing, Visualization, Investigation. **Andreas Kappler:** Writing – review & editing, Supervision, Resources, Project administration, Funding acquisition. **E. Marie Muehe:** Writing – review & editing, Writing – original draft, Validation, Supervision, Resources, Project administration, Funding acquisition, Conceptualization.

Declaration of competing interest

The authors declare that they have no known competing financial interests or personal relationships that could have appeared to influence the work reported in this paper.

Acknowledgements

We appreciate and are thankful for the support we received from the Swedish Polar Research Secretariat and SITES at the Abisko Research Station (Abisko, Sweden). We thank K. Lenge, S. Keldenich, F. Schädler,

L. Grimm, E. Voggenreiter, N. Kainz, and the Geomicrobiology group members for their help in the laboratory. We thank P. Joshi and S. van Grinsven for helpful discussions. We are grateful to C. Schmidt for a first draft of the proposal, which gave good scientific direction. We thank three very thorough and constructive reviewers and editor for improving this manuscript. We further acknowledge financial and infrastructural support by the Deutsche Forschungsgemeinschaft (DFG, German Research Foundation) and proposal number 465839667. E.M. Muehe acknowledges the Helmholtz Young Investigator Grant RhizoThreats.

Appendix A. Supplementary data

Supplementary data to this article can be found online at https://doi.org/10.1016/j.geoderma.2025.117658.

Data availability

The datasets generated during and/or analysed during the current study are also available from the corresponding authors on reasonable request.

References

Agethen, S., Sander, M., Waldemer, C., Knorr, K.-H., 2018. Plant rhizosphere oxidation reduces methane production and emission in rewetted peatlands. Soil Biol. Biochem. 125, 125–135.
Apprill, A., McNally, S., Parsons, R., Weber, L., 2015. Minor revision to V4 region SSU rRNA 806R gene primer greatly increases detection of SAR11 bacterioplankton. Aquat. Microb. Ecol. 75 (2), 129–137.
Bhattacharyya, A., Schmidt, M.P., Stavitski, E., Martínez, C.E., 2018. Iron speciation in peats: chemical and spectroscopic evidence for the co-occurrence of ferric and ferrous iron in organic complexes and mineral precipitates. Org Geochem. 115, 124–137.
Bian, R., Shi, W., Chai, X., Sun, Y., 2020. Effects of plant radial oxygen loss on methane oxidation in landfill cover soil: a simulative study. Waste Manag. 102, 56–64.
Blume-Werry, G., Milbau, A., Teuber, L.M., Johansson, M., Dorrepaal, E., 2019. Dwelling in the deep–strongly increased root growth and rooting depth enhance plant interactions with thawing permafrost soil. New Phytol. 223 (3), 1328–1339.
Bodelier, P.L., 2011. Interactions between nitrogenous fertilizers and methane cycling in wetland and upland soils. Curr. Opin. Environ. Sustain. 3 (5), 379–388.
Boye, K., Noël, V., Tfaily, M.M., Bone, S.E., Williams, K.H., Bargar, J.R., Fendorf, S., 2017. Thermodynamically controlled preservation of organic carbon in floodplains. Nat. Geosci. 10 (6), 415–419.
Chen, C., Dynes, J.J., Wang, J., Sparks, D.L., 2014. Properties of Fe-organic matter associations via coprecipitation versus adsorption. Environ. Sci. Technol. 48 (23), 13751–13759.
Christensen, T.R., 2024. Wetland emissions on the rise. Nat. Clim. Chang. 14 (3), 210–211.
Colmer, T., Voesenek, L., 2009. Flooding tolerance: suites of plant traits in variable environments. Funct. Plant Biol. 36 (8), 665–681.
Duchesneau, K., Riquelme, B.A., Petro, C., Makke, G., Green, M., Tfaily, M., Wilson, R., Roth, S., Johnston, E., Kluber, L., 2025. Northern peatland microbial communities exhibit resistance to warming and acquire electron acceptors from soil organic matter.
Freire-Zapata, V., Holland-Moritz, H., Cronin, D.R., Aroney, S., Smith, D.A., Wilson, R. M., Ernakovich, J.G., Woodcroft, B.J., Bagby, S.C., 13, E.F.T.H.S.B.M.R., 2024. Microbiome–metabolite linkages drive greenhouse gas dynamics over a permafrost thaw gradient. Nat. Microbiol. 9 (11), 2892–2908.
Hattori, S., 2008. Syntrophic acetate-oxidizing microbes in methanogenic environments. Microbes Environ. 23 (2), 118–127.
Haviland, K.A., Noyce, G.L., 2024. Assessing root–soil interactions in wetland plants: root exudation and radial oxygen loss. Biogeosciences 21 (22), 5185–5198.
Hütsch, B.W., Augustin, J., Merbach, W., 2002. Plant rhizodeposition — an important source for carbon turnover in soils. J. Plant Nutr. Soil Sci. 165, 397–407.
Jeannotte, R., 2014. Metabolic pathways| nitrogen metabolism.
Jimenez, J.d.l.C., Pellegrini, E., Pedersen, O., Nakazono, M., 2021. Radial oxygen loss from plant roots—methods. Plants 10 (11), 2322.
Kassambara, A., Mundt, F., 2020. factoextra: Extract and Visualize the Results of Multivariate Data Analyses. R package version 1.0.7. https://CRAN.R-project.org/package=factoextra.
Keiluweit, M., Bougoure, J.J., Nico, P.S., Pett-Ridge, J., Weber, P.K., Kleber, M., 2015. Mineral protection of soil carbon counteracted by root exudates. Nat. Clim. Chang. 5 (6), 588–595.
Krüger, N., Knorr, K.-H., Mueller, P., 2025. Opposite priming responses to labile carbon versus oxygen pulses in anoxic peat. Soil Biol. Biochem. 202, 109682.
Kuzyakov, Y., 2010. Priming effects: interactions between living and dead organic matter. Soil Biol. Biochem. 42 (9), 1363–1371.
Laanbroek, H.J., 2010. Methane emission from natural wetlands: interplay between emergent macrophytes and soil microbial processes. A mini-review. Ann. Botany 105 (1), 141–153.
Lafleur, P.M., 2009. Connecting atmosphere and wetland: trace gas exchange. Geogr. Compass 3 (2), 560–585.
Lamers, L.P., Van Diggelen, J.M., Op den Camp, H.J., Visser, E.J., Lucassen, E.C., Vile, M. A., Jetten, M.S., Smolders, A.J., Roelofs, J.G., 2012. Microbial transformations of nitrogen, sulfur, and iron dictate vegetation composition in wetlands: a review. Front. Microbiol. 3, 156.
Li, H., Bolscher, T., Winnick, M., Tfaily, M.M., Cardon, Z.G., Keiluweit, M., 2021. Simple plant and microbial exudates destabilize mineral-associated organic matter via multiple pathways. Environ. Sci. Technol. 55 (5), 3389–3398.
Li, H., Ye, Z., Wei, Z., Wong, M.H., 2011. Root porosity and radial oxygen loss related to arsenic tolerance and uptake in wetland plants. Environ. Pollut. 159 (1), 30–37.
Li, J., Zhang, H., Xie, W., Liu, C., Liu, X., Zhang, X., Li, L., Pan, G., 2024. Elevated CO2 increases soil redox potential by promoting root radial oxygen loss in paddy field. J. Environ. Sci. 136, 11–20.
Lovley, D.R., Phillips, E.J., 1987. Competitive mechanisms for inhibition of sulfate reduction and methane production in the zone of ferric iron reduction in sediments. Appl. Environ. Microbiol. 53 (11), 2636–2641.
Lueders, T., Manefield, M., Friedrich, M.W., 2004. Enhanced sensitivity of DNA-and rRNA-based stable isotope probing by fractionation and quantitative analysis of isopycnic centrifugation gradients. Environ. Microbiol. 6 (1), 73–78.
Määttä, T., Malhotra, A., 2024. The hidden roots of wetland methane emissions. Glob. Chang. Biol. 30 (2), e17127.
Maisch, M., Lueder, U., Kappler, A., Schmidt, C., 2020. From plant to paddy—how rice root iron plaque can affect the paddy field iron cycling. Soil Systems 4 (2), 28.
Meier, A.B., Oppermann, S., Drake, H.L., Schmidt, O., 2021. Organic carbon from graminoid roots as a driver of fermentation in a fen. FEMS Microbiol. Ecol. 97 (11), fiab143.
Monteux, S., Weedon, J., Blume-Werry, G., Gavazov, K., Jassey, V., Johansson, M., Keuper, F., Olid, C., Dorrepaal, E., 2018. Long-term in situ permafrost thaw effects on bacterial communities and potential aerobic respiration. ISME J. 12 (9), 2129–2141.
Mueller, P., Megonigal, J.P., 2024. Redox control on rhizosphere priming in wetlands. Nat. Geosci. 17 (12), 1209–1217.
Noyce, G.L., Smith, A.J., Kirwan, M.L., Rich, R.L., Megonigal, J.P., 2023. Oxygen priming induced by elevated CO2 reduces carbon accumulation and methane emissions in coastal wetlands. Nat. Geosci. 16 (1), 63–68.
Oburger, E., Jones, D.L., 2018. Sampling root exudates–mission impossible? Rhizosphere 6, 116–133.
Parada, A.E., Needham, D.M., Fuhrman, J.A., 2016. Every base matters: assessing small subunit rRNA primers for marine microbiomes with mock communities, time series and global field samples. Environ. Microbiol. 18 (5), 1403–1414.
Patzner, M.S., Mueller, C.W., Malusova, M., Baur, M., Nikeleit, V., Scholten, T., Hoeschen, C., Byrne, J.M., Borch, T., Kappler, A., 2020. Iron mineral dissolution releases iron and associated organic carbon during permafrost thaw. Nat. Commun. 11 (1), 6329.
Posit team (2024). RStudio: Integrated Development Environment for R. Posit Software, PBC, Boston, MA. URL http://www.posit.co/.
R Core Team, 2024. R: A Language and Environment for Statistical Computing. R Foundation for Statistical Computing, Vienna, Austria. https://www.R-project.org/.
Reddy, K.R., DeLaune, R.D., Inglett, P.W., 2022. Biogeochemistry of Wetlands: Science and Applications. CRC Press.
Ruser, R., Schilling, R., Steindl, H., Flessa, H., Beese, F., 1998. Soil compaction and fertilization effects on nitrous oxide and methane fluxes in potato fields. Soil Sci. Soc. Am. J. 62 (6), 1587–1595.
Slowikowski, K.. ggrepel: Automatically Position Non-Overlapping Text Labels with 'ggplot2'. R package version 0.9.6. https://CRAN.R-project.org/package=ggrepel.
Stookey, L., 1970. Ferrozine - a new sprectrophotometric reagent for iron. Anal. Chem. 42 (7), 779–781.
Sun, H., Ma, X., Van Zwieten, L., Luo, Y., Brown, R.W., Guggenberger, G., Tang, S., Kuzyakov, Y., Jeewani, P.H., 2025. Iron oxides promote physicochemical stabilization of carbon despite enhancing microbial activity in the rice rhizosphere. Sci. Total Environ. 958, 178019.
Sutton-Grier, A.E., Megonigal, J.P., 2011. Plant species traits regulate methane production in freshwater wetland soils. Soil Biol. Biochem. 43 (2), 413–420.
Tanner, C.C., 2001. Plants as ecosystem engineers in subsurface-flow treatment wetlands. Water Sci. Technol. J. Int. Assoc. Water Pollut. Res. 44 (11–12), 9–17.
Teh, Y.A., Silver, W.L., Conrad, M.E., 2005. Oxygen effects on methane production and oxidation in humid tropical forest soils. Glob. Chang. Biol. 11 (8), 1283–1297.
Van Bodegom, P.M., Scholten, J.C., Stams, A.J., 2004. Direct inhibition of methanogenesis by ferric iron. FEMS Microbiol. Ecol. 49 (2), 261–268.
Verhoeven, J.T., Sorrell, B.K., 2010. Plant adaptations and microbial processes in wetlands. Ann. Bot. 105 (1), 127.
Vogel, D., 2017. Colonization of the rice rhizosphere by microbial communities involved in the syntrophic degradation of rhizodeposits to methane.
Voggenreiter, E., Schmitt-Kopplin, P., ThomasArrigo, L., Bryce, C., Kappler, A., Joshi, P., 2024. Emerging investigator series: preferential adsorption and coprecipitation of permafrost organic matter with poorly crystalline iron minerals. Environ. Sci. Processes Impacts 26 (8), 1322–1335.
Waldo, N.B., Hunt, B.K., Fadely, E.C., Moran, J.J., Neumann, R.B., 2019. Plant root exudates increase methane emissions through direct and indirect pathways. Biogeochemistry 145 (1–2), 213–234.
Wang, C., Kuzyakov, Y., 2024. Soil organic matter priming: the pH effects. Glob. Chang. Biol. 30 (6), e17349.

Wei, L., Zhu, Z., Razavi, B.S., Xiao, M., Dorodnikov, M., Fan, L., Yuan, H., Yurtaev, A., Luo, Y., Cheng, W., 2022. Visualization and quantification of carbon "rusty sink" by rice root iron plaque: mechanisms, functions, and global implications. Glob. Chang. Biol. 28 (22), 6711–6727.

Weiss, J.V., Emerson, D., Backer, S.M., Megonigal, J.P., 2003. Enumeration of Fe (II)-oxidizing and Fe (III)-reducing bacteria in the root zone of wetland plants: implications for a rhizosphere iron cycle. Biogeochemistry 64 (1), 77–96.

Wickham, H., 2016. ggplot2: Elegant Graphics for Data Analysis. Springer-Verlag, New York.

Wild, B., Gentsch, N., Čapek, P., Diáková, K., Alves, R.J.E., Bárta, J., Gittel, A., Hugelius, G., Knoltsch, A., Kuhry, P., 2016. Plant-derived compounds stimulate the decomposition of organic matter in arctic permafrost soils. Sci. Rep. 6 (1), 25607.

Wild, B., Monteux, S., Wendler, B., Hugelius, G., Keuper, F., 2023. Circum-Arctic peat soils resist priming by plant-derived compounds. Soil Biol. Biochem. 180, 109012.

Wilmoth, J.L., Schaefer, J.K., Schlesinger, D.R., Roth, S.W., Hatcher, P.G., Shoemaker, J. K., Zhang, X., 2021. The role of oxygen in stimulating methane production in wetlands. Glob. Chang. Biol. 27 (22), 5831–5847.

Yazbeck, T., Bohrer, G., 2023. Uncertainties in wetland methane-flux estimates. Glob. Chang. Biol. 29 (15).

York, L.M., Carminati, A., Mooney, S.J., Ritz, K., Bennett, M.J., 2016. The holistic rhizosphere: integrating zones, processes, and semantics in the soil influenced by roots. J. Exp. Bot. 67 (12), 3629–3643.

Zhu, E., Liu, Z., Wang, S., Wang, Y., Liu, T., Feng, X., 2023. Organic carbon and lignin protection by metal oxides versus silicate clay: Comparative study based on wetland and upland soils. J. Geophys. Res. Biogeo. 128 (7), e2023JG007474.